Stochastic resonance on excitable small-world networks via a pacemaker

Matjaž Perc*
Department of Physics, Faculty of Natural Sciences and Mathematics, University of Maribor, Koroška cesta 160, SI-2000 Maribor, Slovenia

(Received 4 August 2007; revised manuscript received 30 September 2007; published 11 December 2007)

We show that the correlation between the frequency of subthreshold pacemaker activity and the response of an excitable array is resonantly dependent on the intensity of additive spatiotemporal noise. Thereby, the effect of the underlying network, defining the interactions among excitable units, largely depends on the coupling strength. Only for intermediate coupling strengths is the small world property able to enhance the stochastic resonance, whereas for smaller and larger couplings the impact of the transition from diffusive to random networks is less profound. Thus, the optimal interplay between a localized source of weak rhythmic activity and the response of the whole array demands a delicate balance between the strength of excitation transfer and the effectiveness of the network structure to support it.

DOI: 10.1103/PhysRevE.76.066203 PACS number(s): 05.45.−a, 05.40.−a, 89.75.Hc

I. INTRODUCTION

Noise introduced to nonlinear systems can have a profound effect on their dynamics [1]. Phenomena such as stochastic [2] and coherence [3] resonance have fueled studies across diverse fields of research for over a decade, and yet they still inspire even today. One of the most thoroughly studied features of nonlinear dynamics in this context is excitability, which has been recognized as an important system property for a broad variety of noise-induced phenomena [4]. Upon the impact of weak stimuli an excitable system exhibits large amplitude deviations from the steady state. Neural and cardiac cells are two perhaps most prominent examples of excitable systems [5]. Following initial advances in understanding effects of noise on individual dynamical systems, the scope shifted to coupled arrays [6], where it has been discovered that the spatiality may additionally enhance the phenomena of stochastic [7] and coherence [8] resonance. Recently, however, the field of research focusing on the effects of noise in spatially extended systems [9] is growing so rapidly that we found it impossible to overview here all relevant contributions. Some works published past the date of the previous referral along with a comprehensive review are listed in [10] for guidance.

While in the past the majority of scientific research dealing with the dynamics of spatially extended systems was devoted to the study of regular diffusively coupled networks, recently the focus has been shifting towards networks with more complex topologies [11]. Since already a small fraction of randomly introduced links between distant units largely decreases the typical path length between two arbitrary sites, such networks were termed appropriately as "small-world" networks [12]. Importantly, networks with small-world properties appear to be excellent for modeling interactions among units of complex systems. Examples range from social networks [13], scientific-collaboration networks [14], food webs [15], computer networks [16], and of particular interest for the present paper, also to neural and excitable networks in general [17].

Stochastic [18] and coherence [19] resonance phenomena were already studied in networks with small-world topology. In general, it has been reported that the introduction of shortcut links between randomly chosen units increases the order of the dynamics, whereby the ordering effect depends largely on the coupling strength and the fraction of rewired links. Moreover, pattern formation and spatial order of spiral waves in media with small-world connections have also been studied [20], as were regularization effects of complex topologies and their ability to suppress spatiotemporal chaos [21] or induce bursting oscillations [22].

Presently, we wish to extend the scope of stochastic resonance in small-world networks by studying its emergence in the presence of subthreshold pacemaker activity. Pacemakers are isolated cells in the tissue that dictate neighboring cells the operating rhythm, i.e., pace, and so guide the functioning of a larger ensemble. Probably the most prominent organ that has pacemaker cells is the human heart [23]; but also many arteries and arterioles, for example, exhibit rhythmical contractions that are synchronous over considerable distances [24]. A well-known network of pacemaker cells are also the so-called interstitial cells of Cajal (ICC), which regulate the contractility of many smooth muscle cells in several organs, particularly in the gastrointestinal tract [25] and the urethra [26]. Recently, noncontractile cells closely resembling ICC were identified also in the wall of portal veins and mesenteric arteries [27]. Moreover, it should be noted that pacemakers are not characteristic only for whole organs or tissue, but may also be encountered in larger cells like eggs, where cortical endoplasmic reticulum rich clusters act as pacemaker sites dedicated to the initiation of global calcium waves, which then propagate throughout the egg [28].

Due to the considerable importance of pacemakers in real-life systems, some studies were already devoted to their impact on excitable systems [29], as well as on networks with small-world topology [30]. To extend the subject, we study the possibility of stochastic resonance on excitable small-world networks via a pacemaker. More precisely, we intro-

*Mailing address: University of Maribor, Department of Physics, Faculty of Natural Sciences and Mathematics, Koroška cesta 160, SI-2000 Maribor, Slovenia; FAX: +386 2 2518180; matjaz.perc@uni-mb.si

duce a subthreshold periodic pacemaker to one excitable unit of the network and study how different intensities of spatiotemporal noise affect the correlation between the frequency of the pacemaker and the temporal output of the whole array. We find that there exists an optimal intensity of noise for which this correlation is maximal, thus indicating the existence of pacemaker-driven stochastic resonance in the studied excitable array. Thereby, the excitable units are modeled by a discrete map recently proposed by Rulkov [31], and the couplings between them obey the topology of networks proposed by Watts and Strogatz [12]. We show that the ability of network topology to influence the stochastic resonance depends significantly on the coupling strength, which indicates that the optimal interplay between a localized source of weak rhythmic activity and the temporal response of the whole array demands a delicate balance between the strength of excitation transfer and the effectiveness of the network structure to support it. In particular, we demonstrate that, provided the coupling strength is adequately adjusted, the optimal topology for pacemaker-driven stochastic resonance can be determined by the ratio between the normalized clustering coefficient and the characteristic path length [12] of the underlying small-world network.

II. MATHEMATICAL MODEL AND SETUP

We use a two-dimensional excitable map describing neural dynamics [31] that reproduces all the main features of more complex models [5], but allows a numerically efficient treatment of systems with spatial degrees of freedom. The map, along with the Gaussian noise and the coupling term, takes the form

$$u_{n+1}^{(i)} = \alpha/(1+u_n^{(i)2}) + v_n^{(i)} + \sigma\xi_n^{(i)} + \sum_j \varepsilon_{ij}(u_n^{(j)} - u_n^{(i)}), \quad (1)$$

$$v_{n+1}^{(i)} = v_n^{(i)} - \beta u_n^{(i)} - \gamma, \quad (2)$$

where the neuron cell membrane voltage $u_n^{(i)}$ and the variation of ion concentration near the neuron membrane $v_n^{(i)}$ are considered as dimensionless variables, n is the discrete time index, subscripts in brackets enumerate coupled units, σ^2 is the variance of Gaussian noise satisfying $\langle\xi_n\rangle=0$ and $\langle\xi_n^{(i)}\xi_m^{(j)}\rangle=\delta_{nm}\delta_{ij}$, ε_{ij} is the coupling strength between units i and j, while α, β, and γ are system parameters. The main system parameter is α, while β and γ essentially act as time scaling parameters for the variable $v_n^{(i)}$. By choosing $\beta=\gamma=0.001\ll 1$, we achieve that $v_n^{(i)}$ changes slowly in comparison to $u_n^{(i)}$. For $\alpha<2.0$ each excitable unit is governed by a single excitable steady state (u^*,v^*) that can be derived analytically by setting $u_n=u_{n+1}$ and $v_n=v_{n+1}$ in an individual map. Thereby, we obtain $u^*=-1$ and $v^*=-1-(\alpha/2)$. By setting $\alpha=1.95$, each unit thus occupies the excitable steady state $(u^*,v^*)=(-1,-1.995)$, which are also the initial conditions we will use in all subsequent calculations. These imply that the whole network remains forever quiescent if $\sigma=0$.

The coupling strength ε_{ij} depends on the underlying interaction network, which we obtain via the procedure described in [12] by starting from a regular ring with periodic boundary conditions comprising $N=300$ vertices, each having $k=6$ nearest neighbors as shown in Fig. 1(a). The probability of rewiring a link is denoted by p and can occupy any value from the unit interval, whereby $p=0$ constitutes a regular graph (the initial configuration does not change) while $p=1$ results in a random network. For $0<p<1$, as exemplified in Fig. 1(b), the resulting network may have small-world properties in that the normalized characteristic path length L between distant units is small, i.e., comparable with that of a random network, while the normalized clustering coefficient C is still large, i.e., comparable with that of a regular nearest-neighbor graph. According to [12], the characteristic path length is defined as the average number of edges in the shortest path between any two vertices, while the clustering coefficient is the average fraction of all $k_i(k_i-1)/2$ allowable edges that actually exist among vertex i and all its k_i neighbors. If vertices (in our case excitable units) i and j are connected then $\varepsilon_{ij}=\varepsilon_{ji}=\varepsilon$, but otherwise $\varepsilon_{ij}=\varepsilon_{ji}=0$. Furthermore, $\varepsilon_{ii}=0$ and no vertices are allowed to become disconnected from the network during the rewiring procedure.

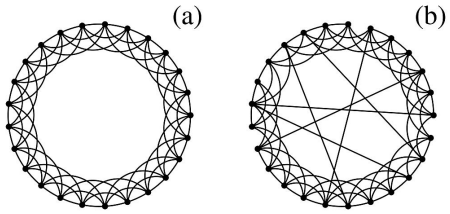

FIG. 1. Examples of considered network topologies. For clarity regarding the meaning of parameters k and p only 25 vertices are displayed in each panel. (a) Regular ring characterized by $p=0$ with periodic boundary conditions. Each vertex is connected to its $k=6$ nearest neighbors. (b) Realization of small-world topology via random rewiring of a certain fraction p of links (in this case 6 out of all 150 were rewired, hence $p=0.04$).

It remains of interest to mathematically introduce the pacemaker. The latter takes the form of a periodic spike train defined by

$$\pi_n^{(r)} = \begin{cases} g & \text{if} \quad (n \bmod t) \geq (t-w) \\ 0 & \text{else} \end{cases}, \quad (3)$$

where t is the oscillation period of the pacemaker, w is the width and g the amplitude of each pulse, respectively. Moreover, the subscript r denotes a randomly chosen excitable unit among all the $N=300$ units constituting the excitable array, to which the pacemaker is introduced as an additive term to the variable $u_n^{(r)}$. For our numerical simulations we choose the parameter values $t=1000$, $w=50$, and $g=0.0025$, which warrant that without the introduction of noise ($\sigma=0$) the pacemaker is subthreshold, meaning it cannot by itself induce large-amplitude excitations by any of the excitable units.

For each set of values ε, p, and σ the temporal output of each excitable unit given by the variable $u_n^{(i)}$ is recorded for $T=300$ periods of the pacemaker, and the correlation of each

series with the frequency of the pacemaker $\omega=2\pi/t$ is computed via the Fourier coefficients $Q^{(i)}$ according to [32]

$$Q_{\sin}^{(i)} = \frac{2}{Tt}\sum_{n=1}^{Tt} u_n^{(i)} \sin(\omega n), \tag{4}$$

$$Q_{\cos}^{(i)} = \frac{2}{Tt}\sum_{n=1}^{Tt} u_n^{(i)} \cos(\omega n), \tag{5}$$

$$Q^{(i)} = \sqrt{Q_{\sin}^{(i)2} + Q_{\cos}^{(i)2}}. \tag{6}$$

Since the Fourier coefficients are exactly proportional to the (square of the) spectral power amplification [33], which is frequently used as a measure for stochastic resonance, the signal-to-noise ratio $\tilde{S}$ is computed as the average value of all $Q^{(i)}$, i.e., $\tilde{S}=N^{-1}\Sigma_{i=1}^{N}Q^{(i)}$. Importantly, the final signal-to-noise ratio S presented in the figures below is obtained by averaging $\tilde{S}$ over 100 different realizations of each network and randomly chosen values of r (network unit to which the pacemaker is introduced). Although in principal the connectivity of the unit to which the pacemaker is introduced could play an important role, our calculations indicate that the intuitive reasoning, suggesting a pacemaker should be more effective if introduced to a unit with a higher connectivity, does not prevail (at least not by small-world networks as proposed in [12]) because the overall dissipation of connectivity around the mean (in our case $k=6$) remains fairly small even if p is close to 1. This is especially so in comparison to scale-free networks [11], where the connectivity of the unit to which the pacemaker is introduced is likely to be found more important.

III. RESULTS

In what follows, we will systematically analyze effects of different ε, p, and σ on the noise-induced temporal dynamics of the array. First, we consider four space-time plots obtained for different σ by fixed ε and p. Results presented in Fig. 2 evidence that the temporal dynamics of each excitable unit follows the rhythm of the pacemaker optimally only by an intermediate σ (second panel from top). Smaller σ (top panel) fail to evoke any large-amplitude excitations, while larger σ (bottom two panels) introduce spontaneous excitations that are either no longer in accord with the pacemaker frequency (third panel from top) or lack visible spatiotemporal order altogether (bottom panel).

It is, however, interesting to note that values of σ beyond the one warranting optimal correlation (so far according to visual inspection) with the pacemaker may still evoke very ordered periodic fronts that even surpass the regularity of their predecessors evoked by smaller σ, as exemplified in the third panel from the top in Fig. 2. Indeed, by introducing a measure for the degree of spatial synchronization

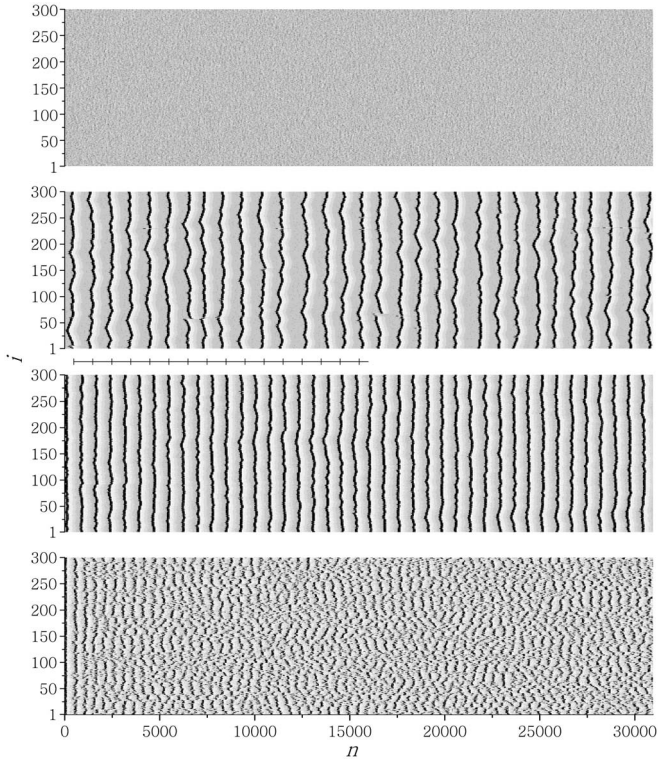

FIG. 2. Space-time plots obtained by $\sigma=0.004$ (top panel), $\sigma=0.008$ (second panel from top), $\sigma=0.016$ (third panel from top), and $\sigma=0.07$ (bottom panel). The pacemaker has been introduced to the network unit $r=150$, but results remain qualitatively the same if the pacemaker is introduced elsewhere on the network. Vertical ticks on the line inserted between the middle two panels denote consecutive pacemaker pulses for easier comparisons. Other parameter values are $\varepsilon=0.004$ and $p=0.1$, while already mentioned parameters that are held constant throughout this work are $\alpha=1.95$, $\beta=\gamma=0.001$, $t=1000$, $w=50$, $g=0.0025$, and $k=6$. In all panels the color profile is linear, white depicting -1.6 and black depicting 0.0 values of $u_n^{(i)}$ (in the top panel this scale is divided by a factor of 10 to enable the color coding of small-amplitude deviations from the excitable steady states).

$$\rho = \frac{1}{Tt}\sum_{n=1}^{Tt}[\langle u_n^{(i)2}\rangle - \langle u_n^{(i)}\rangle^2], \tag{7}$$

where $\langle\cdots\rangle$ denote averages over all $i=1,\ldots,N$ coupled units, one can establish that the most synchronized fronts of excitation appear by values of σ that are often beyond those warranting largest S (as will be reported below). Figure 3 features results obtained via Eq. (7), and it can be observed nicely that the lowest value of ρ, characterizing the most synchronous activity of all coupled units ($\rho=0$ if the synchronization would be perfect), is obtained by $\sigma=0.017$, which substantially exceeds $\sigma=0.008$ warranting the best correlation of excitation fronts with the pacemaker depicted in the second panel from the top of Fig. 2. This phenomenon is due to the fact that larger intensities of noise σ may overrule the pacemaker activity and induce spontaneous excitations irrespective of the locally imposed deterministic rhythm. The remarkable order of periodic fronts evoked even

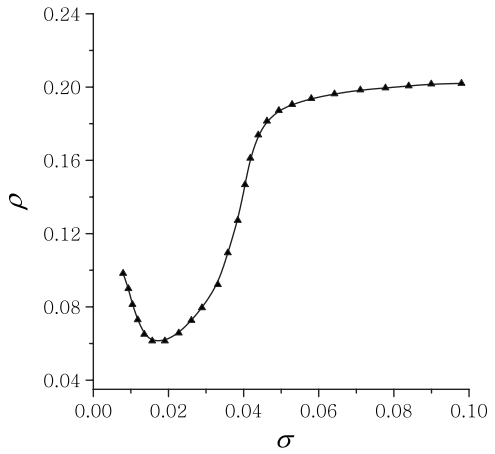

FIG. 3. Degree of spatial synchronization ρ in dependence on σ. All other parameters have the same values as in Fig. 2.

by these larger σ must be attributed to the characteristic noise-robust excursion time inherent to all excitable systems [34], which introduces an eigenfrequency of spatial excitatory events that prevails despite the presence of pacemaker activity. For even larger values of σ, however, also the excursion phase of excitable dynamics becomes blurred, eventually leading to the collapse of ordered periodic fronts, as depicted in the bottom panel of Fig. 2, and consequently, to an increase of ρ as shown in Fig. 3. This phenomenon has already been studied quite extensively and is the underpinning for so-called persistent noise-induced spatial periodicity as well as spatial coherence resonance in excitable media [35]. The interested reader is referred to these works for further heuristic as well as some analytical arguments supporting our above reasoning. Presently though, we wish to focus on the correlation between the subthreshold signal and the system's response as the measure for the constructive effect of different intensities of noise, whereby then results presented in Fig. 2 exemplify a stochastic resonance phenomenon that is driven by a subthreshold pacemaker.

To establish the pacemaker-driven stochastic resonance more precisely, we consider the dependence of S on p and σ by three different ε. Results presented in Fig. 4 show several interesting features. First, it is evident that there indeed exists an intermediate value of σ by which S is maximal for each particular value of p and ε, thus confirming the existence of pacemaker-driven stochastic resonance in the studied system. Second, it appears that an appropriate degree of small-world topology p is able to enhance the stochastic resonance (increase the maximal peak of S) only for an intermediate value of ε (middle panel), while for smaller (left panel) and larger (right panel) ε the effect of topology is limited to shifting the peak value of S with respect to σ but does not noticeably effect the maximal peak height. At $\varepsilon=0.005$ the optimal small-world topology appears to be characterized by $p=0.09$, as will be confirmed also below via results presented in Fig. 5. Finally, perhaps the subtlest observation is that the shift of the maximal S with respect to σ changes direction when $p\to 1$ by small and large ε, as can be inferred from comparing results in the left and right panel of Fig. 4. In particular, for small ε larger σ are required for the maximal S as $p\to 1$, while for large ε the effect of different topologies is exactly opposite.

In order to provide a better quantitative view of the results presented in Fig. 4, we plot S separately in dependence on p (by a given σ), and in dependence on σ (by a given p), for the three considered ε. Figure 5 features results that strengthen the decisive role of ε in that a resonance dependence of S on p, as well as the best-pronounced increase of S by the optimal σ, can be observed by an intermediate value of the coupling strength equaling $\varepsilon=0.005$. In the latter case S by the optimal $p=0.09$ is two times larger than the plateau by smaller p, while for smaller and larger ε the effect of different topologies is mostly cosmetic, as can be inferred from the top panel of Fig. 5. Similarly, results presented in the bottom panel of Fig. 5 evidence that the impact of σ is best expressed by $\varepsilon=0.005$, although also by smaller and larger values of ε the stochastic resonance is clearly visible due to the existence of an intermediate value of σ by which S is maximal.

Before explaining the features of results presented in Figs. 4 and 5, we study the dependence of S on ε more precisely. Figure 6 shows results obtained by the optimal small-world topology characterized by $p=0.09$. Evidently, there exists an optimal value of the coupling strength, equaling $\varepsilon=0.005$, by

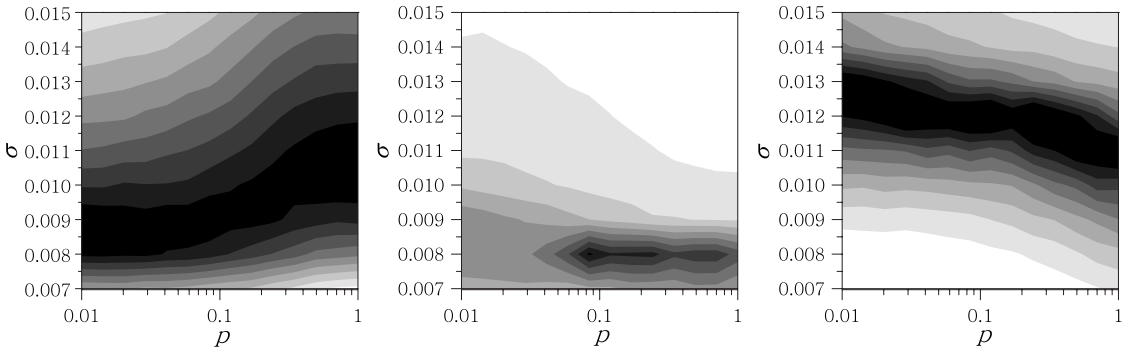

FIG. 4. Color-coded signal-to-noise ratios S in dependence on p and σ by $\varepsilon=0.002$ (left panel), $\varepsilon=0.005$ (middle panel), and $\varepsilon=0.012$ (right panel). In all panels the color profile is linear, white depicting smallest and black depicting largest values of S. The specific intervals of S are 0.0–0.011 (left panel), 0.0–0.024 (middle panel), and 0.0–0.012 (right panel). All other parameters have the same values as in Fig. 2.

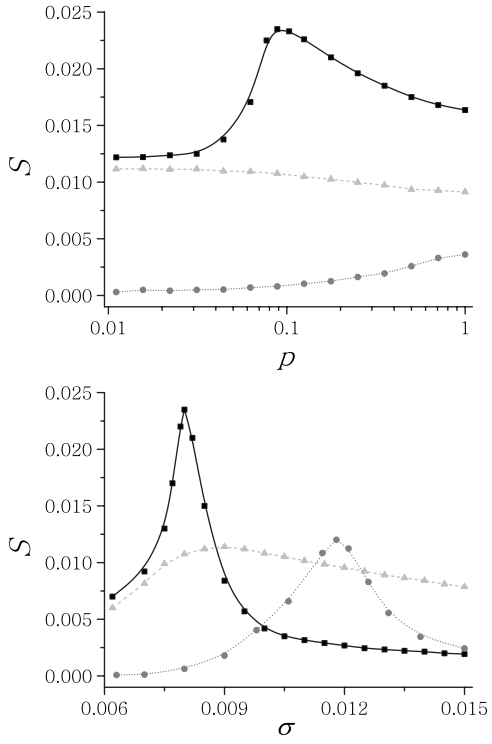

FIG. 5. Signal-to-noise ratios S in dependence on p by $\sigma=0.008$ (top panel), and in dependence on σ by $p=0.09$ (bottom panel) for $\varepsilon=0.002$ (triangles), $\varepsilon=0.005$ (squares), and $\varepsilon=0.012$ (circles). All other parameters have the same values as in Fig. 2, and lines are solely guides to the eye.

which the peak value of S is obtained by the smallest standard deviation of noise. Due to the fact that, in comparison to other values of ε, the smallest σ warrants the resonant peak of S by $\varepsilon=0.005$, this signal-to-noise ratio also represents the maximal overall peak in the whole range of ε and σ covered in Fig. 6, as can be inferred nicely from the inset depicting a resonancelike dependence of the maximally attainable S (resulting out of all σ considered in the main panel of Fig. 6) in dependence on ε. In view of all so far presented results, we conclude that ε plays a key role in determining the ability of the network structure to enhance the noise-induced outreach of the localized subthreshold pacemaker. In particular, only ε bounded to a rather sharp interval of values seems to warrant the optimal balance between the strength (speed) of excitation transfer and the effectiveness of the network structure to support this transmission across all coupled units.

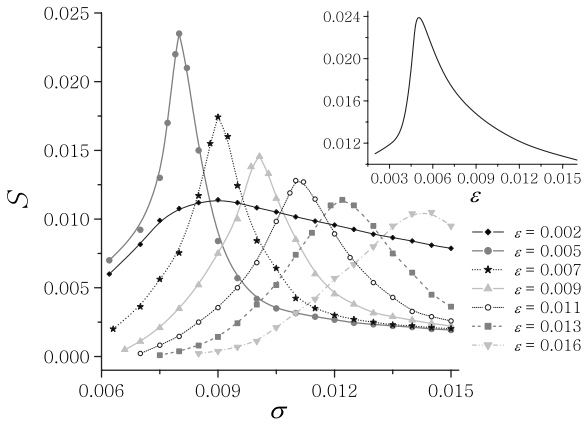

FIG. 6. Signal-to-noise ratios S in dependence on σ and several ε by $p=0.09$. The inset shows the maximally attainable S (peaks in the main panel) in dependence on ε. All other parameters have the same values as in Fig. 2, and lines in the main panel are solely guides to the eye.

In order to explain the presented results, we first make use of the established reasoning suggesting that small ε essentially return the dynamics as would be obtained if all units were detached from each other, and on the other hand, large ε make the whole array act as a single unit. In both cases it is clear that the network structure plays only a side role at most, thus explaining, at least in principal, the rather sharp interval of ε inside which interesting results in dependence on p can be observed. This reasoning also explains why for small ε larger σ are required for the maximal S as $p\to 1$, while for large ε the effect of different p is exactly opposite. In particular, while for large ε additional long-range couplings effectively disperse the pacemaker emitted excitations throughout the array, resulting in smaller optimal σ as p increases, by small ε the long-range couplings act destructive since they further diminish the already very weak (due to small ε) excitation transfer from the pacemaker to nearest neighbors, hence requiring ever larger σ for the maximal S as p increases. Note that by small ε the units cannot benefit from long-range connections since the coupling strength is so small that a coherent input from several nearest neighbors is required to excite a quiescent unit, and thus individual couplings, although potentially bridging the physical distance between them, simply cannot be exploited effectively.

Finally, we study specific properties of small-world topologies by different values of p to explain the occurrence of the optimal network structure if the coupling strength is adequately adjusted, as exemplified in the middle panel of Fig. 4 and the top panel of Fig. 5. For this purpose, we employ classical measures such as the normalized characteristic path length L and the normalized clustering coefficient C [12], as defined in Sec. II. While L is often the more appraised quantity (echoing in the name "small-world" describing such networks), the clustering coefficient is presently also crucial since it quantifies to what extent local interactions are intact or broken. In particular, $C=1$ means that the cliquishness of nearest neighbors is perfect, while $C=0$ means that the neighbors connected to a given unit of the network are disconnected from one another. Since the effectiveness of the pacemaker to enforce its rhythm to other units in the network relies both on effective nearest-neighbor interactions (which must be warranted also by an appropriate value of ε as described above) as well as on the ability to reach physically distant units to which excitations might die out via the diffusive route, we propose the ratio between the normalized clustering coefficient and the characteristic path length $R=C/L$ as the crucial quantity defining the optimal properties of a network to facilitate the spreading of localized pacemaker-emitted rhythmic activity. The higher the value of R, the better the network structure is adapted to enforce the pacemaker activity on other network units. A high value of R

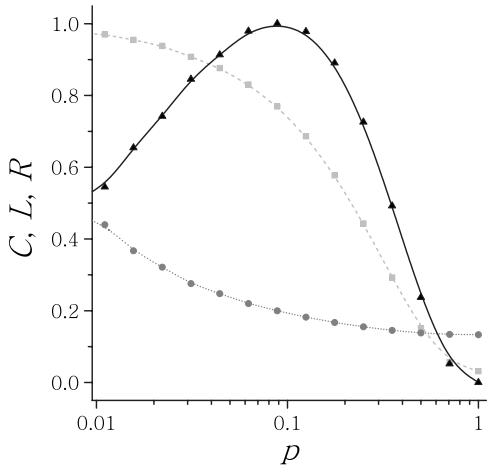

FIG. 7. Normalized clustering coefficient C (squares), normalized characteristic path length L (circles), and the ratio $R=C/L$ (triangles) in dependence on p for a network consisting of $N=300$ vertices having average connectivity $k=6$. Results were averaged over 50 different realizations of each network, and the ratio R was uniformly rescaled to the unit interval (the shape of the dependence on p was completely preserved) for better comparisons of all three curves. Lines are solely guides to the eye.

suggests that the nearest-neighbor interactions are largely intact, while at the same time considerable benefits in terms of excitation propagation may be expected from long-range connections. On the other hand, a low value of R indicates either that nearest-neighbor interactions are largely broken or that long-range connections are sparse, whereby any of these two properties would act detrimental on the ability of a pacemaker to enforce its rhythm on other excitable units in the network. Results for the presently employed network ($N=300$, $k=6$) are shown in Fig. 7. Indeed, the peak value of R is obtained by the same value of the small-world connectivity, equaling $p=0.09$, that also warrants the largest overall S in the middle panel of Fig. 4 and the top panel of Fig. 5. This final result confirms our reasoning and introduces a compact measure for assessing the ability of a network topology to promote the spreading of localized rhythmic activity across coupled units; provided, of course, ε lies within the above-described narrow interval of suitable values. Although presently the analysis was performed for a subthreshold pacemaker in the presence of spatiotemporal noise, the ratio R should prove useful also in case the pacemaker is of supthreshold type.

IV. SUMMARY

We study the impact of subthreshold pacemaker activity on the temporal dynamic of noisy excitable small-world networks. We find that there exists an optimal intensity of spatiotemporal noise by which the correlation between the pacemaker frequency and the temporal output of the whole array is maximal. The pacemaker-driven stochastic resonance can be observed irrespective of p and ε, although several features of the phenomenon depend extensively on the latter two parameters. In particular, for intermediate coupling strengths there exists an optimal small-world topology, warranting the largest peak value of the signal-to-noise ratio, which is determined by the ratio between the normalized clustering coefficient and the characteristic path length of the network. For coupling strengths outside this rather narrow interval the effect of different network topologies is gentler and conforms to the established reasoning implying that for small ε the excitable units effectively act as detached, while for large ε the network acts as a single excitable element. Due to the rather significant importance of pacemakers in several different organs, tissue, and certain types of cells, as emphasized already in the Introduction, we hope our study will also find applicability in real-life motivated problems and foster the understanding of biological processes that rely on an effective pacemaker for their proper functioning.

ACKNOWLEDGMENT

The author acknowledges support from the Slovenian Research Agency (Grant No. Z1-9629).

[1] W. Horsthemke and R. Lefever, *Noise-Induced Transitions* (Springer-Verlag, Berlin, 1984); P. Hänggi and R. Bartussek, in *Nonlinear Physics of Complex Systems*, edited by J. Parisi, S. C. Müller, and W. Zimmermman (Springer, New York, 1999).

[2] R. Benzi, A. Sutera, and A. Vulpiani, J. Phys. A **14**, L453 (1981); C. Nicolis and G. Nicolis, Tellus **33**, 225 (1981); L. Martínez, T. Pérez, C. R. Mirasso, and E. Manjarrez, J. Neurophysiol. **97**, 4007 (2007); E. Manjarrez, I. Mendez, L. Martínez, A. Flores, and C. R. Mirasso, Neurosci. Lett. **415**, 231 (2007); Examples of reviews are P. Jung, Phys. Rep. **234**, 175 (1993); F. Moss, A. Bulsara, and M. F. Shlesinger (editors), J. Stat. Phys. **70**, 1 (1993); L. Gammaitoni, P. Hänggi, P. Jung, and F. Marchesoni, Rev. Mod. Phys. **70**, 223 (1998).

[3] D. Sigeti and W. Horsthemke, J. Stat. Phys. **54**, 1217 (1989); G. Hu Gang, T. Ditzinger, C. Z. Ning, and H. Haken, Phys. Rev. Lett. **71**, 807 (1993); W. J. Rappel and S. H. Strogatz, Phys. Rev. E **50**, 3249 (1994); A. S. Pikovsky and J. Kurths, Phys. Rev. Lett. **78**, 775 (1997); A. Longtin, Phys. Rev. E **55**, 868 (1997).

[4] J. R. Pradines, G. V. Osipov, and J. J. Collins, Phys. Rev. E **60**, 6407 (1999); M. Perc and A. Szolnoki, New J. Phys. **9**, 267 (2007); For a review, see B. Lindner, J. García-Ojalvo, A. Neiman, and L. Schimansky-Geier, Phys. Rep. **392**, 321 (2004).

[5] A. L. Hodgkin and A. F. Huxley, J. Physiol. (London) **117**, 500 (1952); J. Rinzel and G. B. Ermentraut in *Analysis of Neural Excitability and Oscillations. Methods in Neuronal Modeling*, edited by C. Koch and I. Segev (The MIT Press, Cambridge, 1989); C. H. Luo and Y. Rudy, Circ. Res. **74**, 1071 (1994); **74**, 1097 (1994); For a review see, E. M.

Izhikevich, Int. J. Bifurcation Chaos Appl. Sci. Eng. **10**, 1171 (2000).
[6] H. S. Wio, Phys. Rev. E **54**, R3075 (1996).
[7] J. F. Lindner, B. K. Meadows, W. L. Ditto, M. E. Inchiosa, and A. R. Bulsara, Phys. Rev. Lett. **75**, 3 (1995); M. Löcher, G. A. Johnson, and E. R. Hunt, *ibid.* **77**, 4698 (1996); J. F. Lindner, B. K. Meadows, W. L. Ditto, M. E. Inchiosa, and A. R. Bulsara, *ibid.* **53**, 2081 (1996); D. R. Chialvo, A. Longtin, and J. Muller-Gerking, *ibid.* **55**, 1798 (1997); N. Sungar, J. P. Sharpe, and S. Weber, Phys. Rev. E **62**, 1413 (2000).
[8] S. K. Han, T. G. Yim, D. E. Postnov, and O. V. Sosnovtseva, Phys. Rev. Lett. **83**, 1771 (1999); A. Neiman, L. Schimansky-Geier, A. Cornell-Bell, and F. Moss, *ibid.* **83**, 4896 (1999); C. S. Zhou, J. Kurths, and B. Hu, *ibid.* **87**, 098101 (2001).
[9] J. García-Ojalvo and J. M. Sancho, *Noise in Spatially Extended Systems* (Springer, New York, 1999).
[10] J. Wang, Chem. Phys. Lett. **339**, 357 (2001); H. Busch and F. Kaiser, Phys. Rev. E **67**, 041105 (2003); E. Ullner, A. A. Zaikin, J. García-Ojalvo, and J. Kurths, Phys. Rev. Lett. **91**, 180601 (2003); O. Carrillo, M. A. Santos, J. García-Ojalvo, and J. M. Sancho, Europhys. Lett. **65**, 452 (2004); M. R. Roussel and J. Wang, J. Chem. Phys. **120**, 8079 (2004); C. S. Zhou and J. Kurths, New J. Phys. **7**, 18 (2005); E. Glatt, H. Busch, F. Kaiser, and A. Zaikin, Phys. Rev. E **73**, 026216 (2006); Q. Y. Wang, Q. S. Lu, and G. R. Chen, Europhys. Lett. **77**, 10004 (2007); O. Nekhamkina and M. Sheintuch, Phys. Rev. E **75**, 056210 (2007); For a review, see F. Sagués, J. M. Sancho, and J. García-Ojalvo, Rev. Mod. Phys. **79**, 829 (2007).
[11] R. Albert and A.-L. Barabási, Rev. Mod. Phys. **74**, 47 (2002).
[12] D. J. Watts and S. H. Strogatz, Nature (London) **393**, 440 (1998).
[13] S. Wasserman and K. Faust, *Social Network Analysis* (Cambridge University Press, Cambridge, 1994).
[14] A. F. J. Van Raan, Nature (London) **347**, 626 (1990); P. O. Seglen, J. Am. Soc. Inf. Sci. **43**, 628 (1992); S. Redner, Eur. Phys. J. B **4**, 131 (1998).
[15] K. McCann, A. Hastings, and G. R. Huxel, Nature (London) **395**, 794 (1998).
[16] B. A. Huberman and L. A. Adamic, Nature (London) **401**, 131 (1999); L. A. Adamic, B. A. Huberman, A.-L. Barabási, R. Albert, H. Jeong, and G. Bianconi, Science **287**, 2115 (2000).
[17] L. F. Lago-Fernández, R. Huerta, F. Corbacho, and J. A. Sigüenza, Phys. Rev. Lett. **84**, 2758 (2000); O. Shefi, I. Golding, R. Segev, E. Ben-Jacob, and A. Ayali, Phys. Rev. E **66**, 021905 (2002); A. Roxin, H. Riecke, and S. A. Solla, Phys. Rev. Lett. **92**, 198101 (2004); V. M. Eguíluz, D. R. Chialvo, G. A. Cecchi, M. Baliki, and A. V. Apkarian, *ibid.* **94**, 018102 (2005); V. Volman, I. Baruchi, and E. Ben-Jacob, Phys. Biol. **2**, 98 (2005); P. K. Swain and A. Longtin, in *Stochastic Dynamics of Neural and Genetic Networks*, edited by A. Longtin and P. K. Swain special focus issue of Chaos, 16, 026101 (2006); N. Masuda, M. Okada, and K. Aihara, Neural Comput. **19**, 1854 (2007).
[18] Z. Gao, B. Hu, and G. Hu, Phys. Rev. E **65**, 016209 (2001); H. Hong, B. J. Kim, and M. Y. Choi, *ibid.* **66**, 011107 (2002).
[19] O. Kwon and H.-T. Moon, Phys. Lett. A **298**, 319 (2002); O. Kwon, H.-H. Jo, and H.-T. Moon, Phys. Rev. E **72**, 066121 (2005).
[20] D. He, G. Hu, M. Zhan, W. Ren, and Z. Gao, Phys. Rev. E **65**, 055204(R) (2002); X. Wang, Y. Lu, M. Jiang, and Q. Ouyang, *ibid.* **69**, 056223 (2004); M. Perc, New J. Phys. **7**, 252 (2005).
[21] Y. Gong, B. Xu, Q. Xu, C. Yang, T. Ren, Z. Hou, and H. Xin, Phys. Rev. E **73**, 046137 (2006); D. Q. Wie and X. S. Luo, Europhys. Lett. **78**, 68004 (2007).
[22] T.-H. Tsao and R. Butera, Neural Comput. **18**, 2029 (2006).
[23] A. M. Katz, *Physiology of the Heart* (Kluwer, Philadelphia, 2000).
[24] R. E. Haddock and C. E. Hill, J. Physiol. (London) **566**, 645 (2005).
[25] K. M. Sanders, T. Ördög, S. D. Koh, and S. M. Ward, News Physiol. Sci. **15**, 291 (2000).
[26] G. D. S. Hirst and S. M. Ward, J. Physiol. (London) **550**, 337 (2003).
[27] T. B. Bolton, D. V. Gordienko, O. Povstyan, M. I. Harhun, and V. Pucovsky, Cell Calcium **35**, 643 (2004).
[28] R. Dumollard, J. Caroll, G. Dupont, and C. Sardet, J. Cell. Sci. **115**, 3557 (2002).
[29] Y. Nagai, H. González, A. Shrier, and L. Glass, Phys. Rev. Lett. **84**, 4248 (2000); S. Alonso, I. Sendiña-Nadal, V. Pérez-Muñuzuri, J. M. Sancho, and F. Sagués, *ibid.* **87**, 078302 (2001); M. Gutman, I. Aviram, and A. Rabinovitch, Phys. Rev. E **70**, 037202 (2004); L. B. Smolka, B. Marts, and A. L. Lin, *ibid.* **72**, 056205 (2005); V. Jacquemet, *ibid.* **74**, 011908 (2006); M. Perc and M. Marhl, Phys. Lett. A **353**, 372 (2006); T. R. Chigwada, P. Parmananda, and K. Showalter, Phys. Rev. Lett. **96**, 244101 (2006).
[30] H. Kori and A. S. Mikhailov, Phys. Rev. Lett. **93**, 254101 (2004); F. Radicchi and H. Meyer-Ortmanns, Phys. Rev. E **73**, 036218 (2006); A. J. Steele, M. Tinsley, and K. Showalter, Chaos **16**, 015110 (2006).
[31] N. F. Rulkov, Phys. Rev. Lett. **86**, 183 (2001).
[32] W. H. Press, S. A. Teukolsky, W. T. Vetterling, and B. P. Flannery, *Numerical Recipes in C* (Cambridge University Press, Cambridge, 1995).
[33] L. Holden and T. Erneux, SIAM J. Appl. Math. **53**, 1045 (1993).
[34] A. S. Pikovsky, Z. Phys. B: Condens. Matter **55**, 149 (1984).
[35] M. Perc, Europhys. Lett. **72**, 712 (2005); M. Perc and M. Marhl, Phys. Rev. E **73**, 066205 (2006).